# Automated Routing and Control of Silicon Photonic Switch Fabrics

Andrea Annoni, Emanuele Guglielmi, Marco Carminati, *Member, IEEE,* Stefano Grillanda, Pietro Ciccarella, Giorgio Ferrari, *Member, IEEE,* Marc Sorel, Michael Strain, Marco Sampietro, Andrea Melloni and Francesco Morichetti

***Abstract*— Automatic reconfiguration and feedback controlled routing is demonstrated in an 8×8 silicon photonic switch fabric based on Mach-Zehnder interferometers. The use of non-invasive Contactless Integrated Photonic Probes (CLIPPs) enables real-time monitoring of the state of each switching element individually. Local monitoring provides direct information on the routing path, allowing an easy sequential tuning and feedback controlled stabilization of the individual switching elements, thus making the switch fabric robust against thermal crosstalk, even in the absence of a cooling system for the silicon chip. Up to 24 CLIPPs are interrogated by a multichannel integrated ASIC wire-bonded to the photonic chip. Optical routing is demonstrated on simultaneous WDM input signals that are labelled directly on-chip by suitable pilot tones without affecting the quality of the signals. Neither preliminary circuit calibration nor lookup tables are required, being the proposed control scheme inherently insensible to channels power fluctuations.**

***Index Terms*— Feedback; Integrated Optics; Silicon; Photonic switching systems**

## I. Introduction

The explosive growth of silicon photonics driven by datacenters, sensing, automotive and telecommunication applications demands the development of photonic integrated circuits (PICs) with unprecedented complex architectures. The current technologies already enable device miniaturization and aggregation of many photonic components and functionalities onto the same chip, yet the lack of suitable control technologies is today perceived as a "grand challenge" and major obstacle to the advent of large-scale photonic integrated systems [1-2].

Manuscript received 07/02/2016
The research leading to these results has received funding from the European Union's Seventh Framework Programme (FP7/2007/2013) under grant agreement no. 323734 (Breaking the Barriers on Optical Integration).
A.Annoni, E.Guglielmi, M.Carminati, S.Grillanda, P.Ciccarella, G.Ferrari, M.Sampietro, A.Melloni, F.Morichetti are with the Dipartimento di Elettronica, Informazione e Bioingegneria - Politecnico di Milano, via Ponzio 34/5, Milano,Italy.(e-mail:andrea.annoni@polimi.it; emanuele.guglielmi @polimi.it; marco1.carminati@polimi.it; stefano.grillanda@polimi.it; pietro.ciccarella@polimi.it; giorgio.ferrari @polimi.it; marco.sampietro @polimi.it; andrea.melloni @polimi.it; francesco.morichetti@polimi.it;).
M. Sorel is with the School of Engineering University of Glasgow,Glasgow, G12 8QQ, U.K.(e-mail: Marc.Sorel@glasgow.ac.uk).
M. J. Strain is with the Institute of Photonics, The University of Strathclyde, Glasgow G4 0NW (e-mail: Michael.strain@strath.ac.uk).
Color versions of one or more of the figures in this paper are available online at http://ieeexplore.ieee.org.
Digital Object Identifier

The photonic chip is becoming an increasingly complex system operating in a multiphysical dynamic environment together with electronics, radiofrequency, thermal management and microfluidics and sensing elements. Advanced tools are essential to reliably set, hold, control and steer the desired working point of the system through feedback controlled algorithms [3 – 15].

The possibility to control the PIC is a key requirement for different reasons and in many applications: i) reconfigurability of the circuit to provide the required functionality such as in routers, cross connects, tunable bandwidth filters, reconfigurable add-drop multiplexers, etc.; ii) adaptive circuits that modify their behavior depending on the state of the system such as signal polarization state, signal to noise ratio, crosstalk, eye aperture, BER, etc.; iii) locking or stabilization of the circuit in a well defined state independently of the temperature, electrical fluctuations, drifts, stress, aging, etc; iv) compensation of fabrication tolerances and technological non-uniformities.

All these requirements and aspects become even more critical when dealing with wavelength selective devices, such as microrings resonators, high bit rate signals operating in coherent domain, dense WDM systems and/or with densely integrated PICs realised on a semiconductor photonic platform, such as silicon on insulator (SOI) or indium phosphide (InP). Local and global feedback control tools and strategies will soon become the ordinary way to operate even for simple circuits.

In this paper, we focus on a classical and very well known switch fabric based on silicon Mach-Zehnder interferometers (MZI) [16 - 26]. Although such router is very popular for its geometrical simplicity, its control and stability in real operative conditions with simultaneous multiwavelength signals pose a number of challenges. An 8×8 switch fabric is considered, with feedback-controlled 2×2 switches monitored by 24 CLIPPs in total [27], simultaneously interrogated by an integrated CMOS ASIC enabling to track each light path [28]. Section II describes the circuit architecture and fabrication.

Concerning the organization of the paper, first the automatic tuning and stabilization of a single MZI switch in the maximum or minimum of the transfer function is demonstrated with a robust locking algorithm using a single heater as actuators and CLIPPs as sensing elements providing the feedback signal (Sec. III). The ability of the CLIPP to detect the state of the Mach-Zehnder is exploited to configure the switch fabric in a very

simple and efficient way without the need of lookup tables, as described in Section IV. In case of multiple incoming signals, these are routed using weak pilot tones added at the input ports and read selectively along the router by the CLIPPs. The BER characteristics of two WDM channels OOK modulated at 10Gbit/s are also shown (Sec. V). The locking of the various switching elements guarantees the optimal performance also in presence of thermal and electrical crosstalk that could play a detrimental role on the output optical crosstalk. The active compensation of the mutual thermal crosstalk between switching elements is described in Section VI under both cooled and uncooled conditions.

## II. Circuit Architecture and Fabrication

The photonic circuit employed to demonstrate control and reconfiguration through on-chip light-path tracking is schematically shown in Fig. 1(a). It consists of an 8×8 switch fabric, composed by twelve 2×2 switches realized through thermally-actuated balanced MZIs and arranged in 3 switching stages (*A*, *B*, and *C*). The topology is organized as a butterfly network, but the proposed approach can be generalized to different switch fabric architectures, to larger port counts and, more generally, to any routing/switching photonic integrated circuit. CLIPP detectors are integrated at the output ports of each MZI switch, (thus resulting in 24 CLIPPs in total), enabling to monitor the optical power in each waveguide, without introducing any measurable extra loss or significant perturbation on the optical signal [27].

The silicon channel waveguides employed in the circuit are fabricated by e-beam lithography on a standard 220 nm SOI platform. The waveguide core is 480 nm wide and is buried underneath a 1-µm-thick $SiO_2$ top cladding, that is grown by plasma enhanced chemical vapor deposition (PECVD) [31]. The waveguide propagation loss is 2.5 dB/cm at a wavelength of 1550 nm. Inverse tapers surrounded by SU8 polymer waveguides are realized at the chip edges, reducing coupling loss with lensed optical fiber (1.7 µm spot size) to about 5 dB/facet. Thermal actuators for the MZI switching are realized through 50-µm-long and 900 nm wide Ni/Cr stripes deposited above the $SiO_2$ cladding. Electrical power consumption required to induce a π phase-shift is about 10 mW. The total footprint of the circuit is 1.5 mm × 5.5 mm, including input/output inverse tapers, metallic buses and contact pads. Figure 1(b) shows a top view photograph of a portion of the fabricated circuit, where the two MZI switching stages A and B are visible in the leftmost and rightmost part of the picture, respectively. Between the two MZI stages, the first arrangement of 8 CLIPPs is visible.

The CLIPP detector simply consists of two closely-spaced metal electrodes deposited on top of the silicon waveguide upper cladding [27]. In this circuit, the CLIPPs electrodes have a size of 20 µm × 100 µm and are mutually spaced by 100 µm. Both the CLIPPs' electrodes and the metal connections of the heaters are realized with the same gold layer. Thermal actuator and CLIPP buses are terminated on 100µm x 100µm contact pads, that allows the wire-bonding of the photonic chip to the external electronic circuit.

The CLIPP (Contactless Integrated Photonic Probe) is a simple and inherently CMOS compatible device that monitors

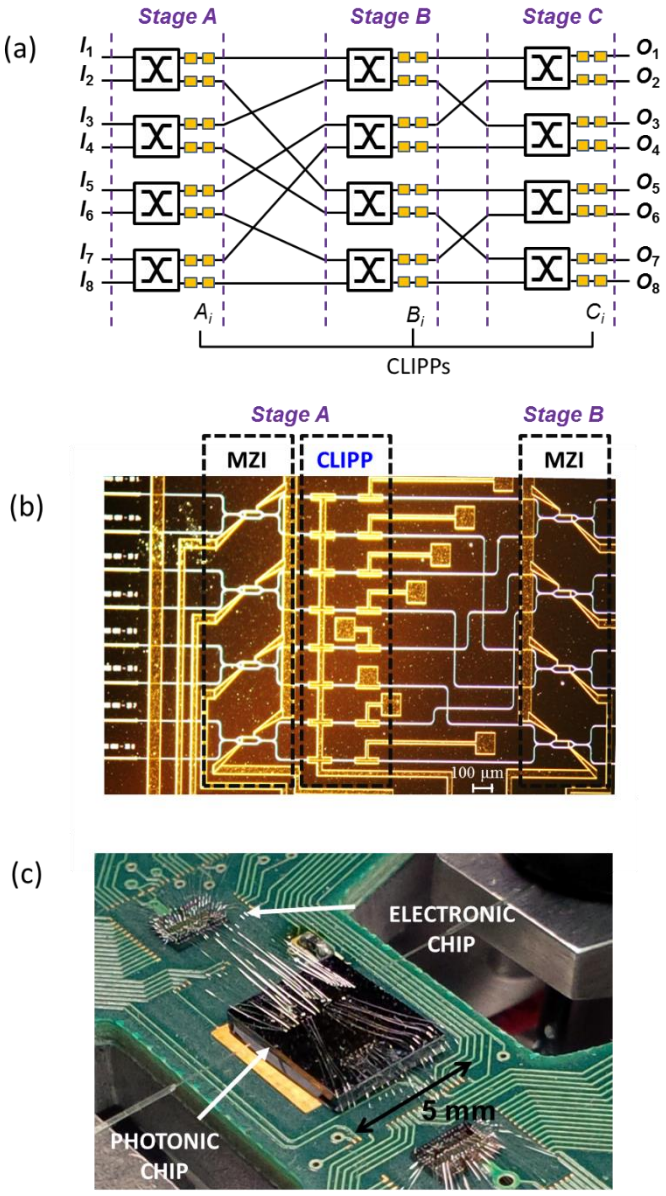


Fig. 1: device used for the experiment. (a) Scheme of the switch fabric, twelve 2x2 switches are arranged in three stages and interconnected. Each switching element is monitored with two CLIPP at its outputs. (b) Top view photograph of a portion of the switch fabric matrix; stages A and B and the first series of CLIPPs are visible. (c) Photo of the Silicon Photonic chip and the two CMOS ASIC mounted onto a PCB, wire bonding allows electrical connections between the chips and the PCB.

the light intensity in the waveguide by measuring the change of the Si core conductance due to sub-band gap generation of free carriers induced by surface state absorption at the core-cladding interface [27]. High sensitivity (-30 dBm), large dynamical range (40 dB), µs scale time response, and negligible perturbation on the optical field enable to use the CLIPP as an in-line transparent monitor to implement feedback loop schemes [29], without introducing measurable degradation of the transmitted signals [30].

As discussed in detail in [27], a CLIPP detector measures the light intensity in the waveguide underneath by measuring the light-induced change of the electric conductivity of the waveguide, which is associated with surface state absorption in

the silicon core. To this aim, one electrode of the CLIPP is driven with a voltage $V_e$ of a few Volts at a frequency $f_e$ in the 100 kHz-1MHz range. Both parameters are adjusted depending on the value of the optical power at the desired working point, in order to maximize the signal-to-noise ratio [29]. At the second electrode a current signal providing information on the light intensity in the waveguide is detected with a low-noise lock-in system [27] implemented on a CMOS electronic circuit [29]. As shown in Fig. 1(b), a common metal bus delivers the driving signal $V_e$ simultaneously to all the CLIPPs of each stage in order to reduce the number of required interconnections.

Simultaneous monitoring of several CLIPPs is performed through a 32-channel ASIC realized in standard CMOS technology and designed to perform low-noise CLIPP signal detection. Details on the design, technology and characterization of the ASIC can be found in [28]. Fig. 1(c) shows how the SiP chip and the ASIC are assembled onto the same printed circuit board (PCB). Since the wiring is very critical from the signal-integrity point-of-view, the CLIPPs are directly bonded to the ASIC in order to reduce parasitics, while the heaters are connected to the PCB.

## III. Feedback Control of MZI Switches

To assess the CLIPP effectiveness to monitor and feedback control the switching state of a silicon MZI, we initially consider only one of the MZIs of stage C. Figure 2(a) shows a top-view photograph of the considered MZI (bottom-most switch of stage C). Here, the optical power at the output ports of the MZI can be directly measured both by using external photodetectors (PDs) and by means of the integrated CLIPPs, thus providing a direct comparison between the two types of detectors. Figs. 2($b_1$-$b_2$) shows, respectively, the normalized light intensity measured in the output waveguides by CLIPPs $C_7$ and $C_8$, and the normalized optical output power $O_7$ and $O_8$ that are simultaneously measured by external PDs for increasing voltage $V_h$ applied to the thermal actuator. The good agreement demonstrates that CLIPPs can provide the same information as conventional PDs on the bias point of an integrated MZI. In this measurement, the wavelength of the laser source is about 1550 nm; at maximum transmission (that is the MZI in ON state), the light intensity in the MZI output waveguide is about -5 dBm.

As shown in Fig. 2(a), the CLIPP signals are sent to an external controller, which modifies the MZI working point by acting on the thermal actuator on one of the two arms of the MZI. In principle, for the routing applications described in this work where the MZI "digitally" operates as an ON (OFF) switch, the control algorithm (with a single degree of freedom represented by $V_h$) only requires a single CLIPP at one of the two output ports, to maximize (minimize) the optical power in the two states. The integration of a CLIPP at both ports, not only can be exploited to increase the control robustness, but also enables to lock the MZI to any intermediate bias condition (such as, for instance, a balanced 50%-50% state), independently of optical power fluctuations at the input port. Real-time closed-loop control is implemented in a programmable digital controller (a 32-bit floating-point RISC processor running at 64 MHz) that directly drives the actuator voltage $V_h$ by means of a 16-bit DAC with a 10 V swing and

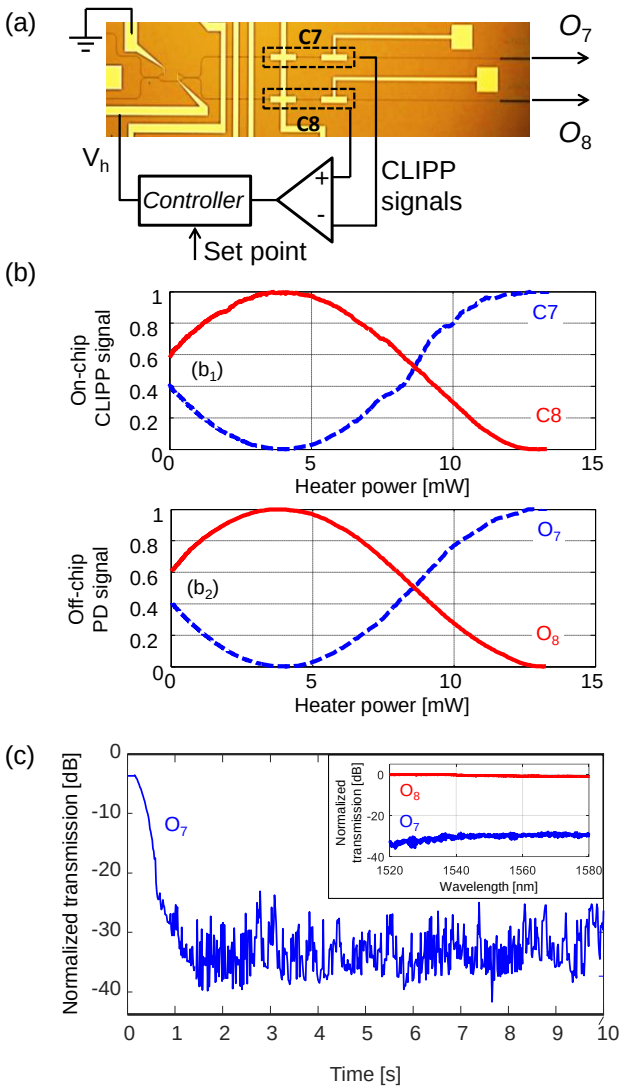


Fig. 2: CLIPP assisted feedback-control of a MZI switch. (a) Top-view photograph of a MZI of the switch fabric (stage *C*). The MZI status is monitored by two CLIPPs placed on the output waveguides; the monitoring signals are used by an external controller to steer the working point of the Mach-Zehnder by acting on the thermo-optical actuator. (b) Comparison between ($b_1$) the electrical signal provided by CLIPPs $C_7$ (dashed blue) and $C_8$ (solid red) at the output of the MZI and ($b_2$) the optical signal simultaneously measured with an external PD at output ports $O_7$ (dashed blue) and $O_8$ (solid red) versus the electrical power dissipated in the thermal actuator. (c) Measured normalized intensity at the output port $O_7$ during the switch OFF of the MZI; the inset shows the steady state normalized spectrum at the output ports $O_7$ (blue, OFF state) and $O_8$ (red, ON state).

acquires the lock-in demodulated CLIPP signals, which are conditioned by the ASIC. The control algorithm is a simple max./min. chaser that can be used to initially tune the MZI to the desired operating point and, if kept active, to compensate for drifts and perturbations by continuously updating $V_h$. The algorithm periodically monitors the CLIPP power level and modifies the actuator driving voltage in steps that are constant in power ($\Delta V_h^2$), in order to uniformly explore the MZI thermal response curve. By comparing the current power level with the previous reading acquired at a different $V_h$, it is possible to determine if the last control voltage adjustment was done in the correct direction. For example, when the minimum is targeted, if a decreasing signal is detected and $V_h$ was increased at the previous step, then the next adjustment is done in the same

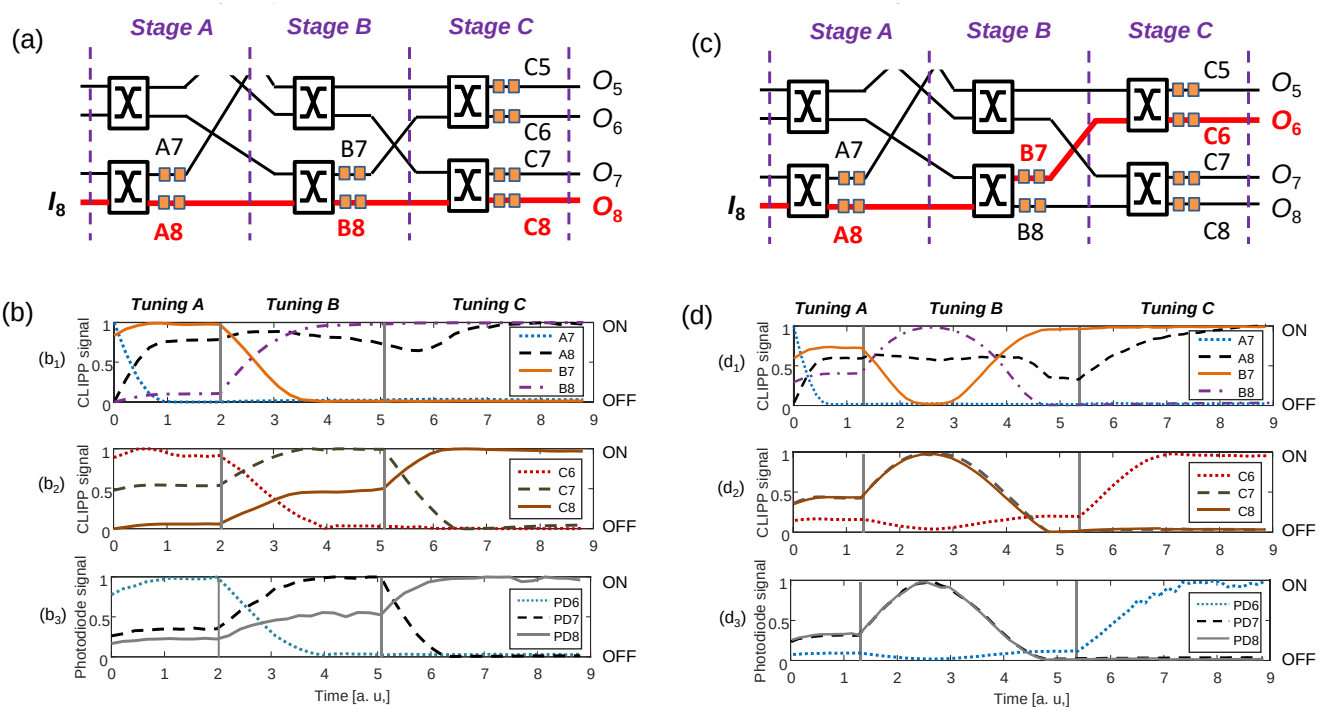


Fig. 3: CLIPP-assisted light-path tracking and circuit reconfiguration. (a) An optical channel from input $I_8$ is routed toward the output $O_8$. (b) The stages of the switch fabric are tuned sequentially by exploiting the information provided by the CLIPPs placed throughout the circuit; ($b_1$) during the tuning of the stage *A*, the signal from CLIPP $A_8$ increases while $A_7$ decreases. $B_7$ and $B_8$ both increases since more power is routed to the fourth MZI of stage *B*; then the second stage is tuned in order to maximize signal from $B_8$. (b3) Signals simultaneously measured by external PDs coupled to the output waveguides during the tuning procedure. Likewise, panels (c) and (d) show routing, light-path tracking and optical intensity at the output ports when input $I_8$ is routed toward output $O_6$.

direction. Fig. 2(c) shows the time-dependent normalized optical power measured with a conventional photodiode at the output port $O_7$, during the CLIPP-assisted switching of the MZI. At the starting point, the heater is switched off ($V_h = 0$) and the output power is about 4 dB below the maximum [see Fig. 2(b)]. At time T = 100 ms, the tuning algorithm is switched on to bring the output port $O_7$ to the OFF state. The optical power level drops by more than 20 dB in about 450 ms and reaches a normalized transmission of less than -30 dB in less than 1 s. Once the minimum transmission is reached, the controller holds the MZI in this state. The closed-loop MZI switching speed is limited by the time response of the CLIPP (set to 8.3 ms by the 120 Hz lock-in filter BW) and by the decision rate of the algorithm (4.4 ms, 225 Sa/s). As detailed in [29], the CLIPP time response can be reduced by increasing the CLIPP driving voltage or the CLIPP size. The residual fluctuations at the MZI output, visible in Fig. 2(c), are due to the locking algorithm that keeps on evaluating the actual operating point. In order to increase the resolution, and thus to reduce the value of $V_h^2$ that produces the residual ripple, the signal can be acquired at a higher sample rate (1.8 kSa/s from 225 Sa/s) and additionally processed with a 256-sample wide moving average filter which increases the decision rate of the algorithm to 200 ms. With these settings, an optimal value of the adjustable $\Delta V_h^2$ has been empirically identified at 20 $mV^2$, as a trade-off between speed, accuracy and residual fluctuations.

## IV. CLIPP ASSISTED LIGHT PATH TRACKING AND CIRCUIT RECONFIGURATION

In this section we discuss the procedure to perform CLIPP-assisted light-path tracking and closed-loop reconfiguration of the 8x8 switching fabric of Fig. 1. For simplicity, we consider the routing of a single optical signal injected from an input port; however, as shown in Sec. V, circuit reconfiguration can be performed even when several optical signals are simultaneously coupled to the input ports of the circuit.

To configure the circuit, we apply a CLIPP-assisted feedback control scheme similar to the one discussed in Sec. III, exploiting both CLIPPs of all the MZIs involved in the routing operations. In this way, each switching element is monitored individually, regardless of the state of the other switches, and can be controlled by means of a simple local feedback loop with a single degree of freedom (e.g. actuator driving voltage). In addition, this method requires neither previous calibrations nor lookup tables, and it is also robust against power fluctuations of the input signals and mutual thermal cross-talk effect, as will be discussed in Sec. VI.

As a first example, we show light routing from input $I_8$ to output $O_8$, according to the schematic of Fig. 3(a). Here a sequential configuration procedure is used, although simultaneous adjustment of different stages can be implemented with more advanced algorithms. At the beginning of the tuning operations all the heaters of the circuit are switched off and hence all the MZIs have random biasing points due fabrication tolerances. Figs. 3($b_1$-$b_2$) show the time-dependent electric signals of the CLIPPs during the circuit

reconfiguration. These signals provide real-time information of the path of the light across the photonic chip. Fig. 3($b_3$) shows the optical signal that is simultaneously acquired by external PDs coupled at output ports $O_6$, $O_7$ and $O_8$.

As a first step (*Tuning A*), stage *A* is tuned to maximize the optical power in the lower output waveguide; this condition is reached when the difference between the signals provided by CLIPP $A_8$ (black dashed line) and CLIPP $A_7$ (blue dotted line) of Fig. 3($b_1$) is maximum. Once stage *A* is tuned, its state is continuously monitored and feedback locked, while the following stages of the circuit are sequentially tuned. In the second step (*Tuning B*), all the power is routed in the lower output waveguide of stage *B*, by maximizing the difference between the signals from CLIPPs $B_8$ (purple dash-dotted line) and $B_8$ (orange solid line). Likewise, the third stage *C* is configured by looking at the signal provided by CLIPPs C7 (grey dashed line) and $C_8$ (brown solid line) of Fig. 3($b_2$).
PD signals of Fig. 3(c) confirm the effectiveness of the CLIPP-assisted reconfiguration procedure. At the end of the tuning operations, the intensity at output ports $O_6$ (cyan dotted line) and $O_7$ (black solid line) is minimized, while all the power is transferred to port $O_8$ (grey solid line). It is worthwhile to note that, even though some information on the current state of the circuit could be inferred from the output PD signals, CLIPP-assisted on-chip local monitoring provides direct information on the status of every single element of the entire architecture. For instance, during the tuning of stage *A*, the three PD outputs $O_6$, $O_7$ and $O_8$ all increase since the MZI is redirecting the light to the lowest four ports of the switch fabric. Therefore, to optimize the working point of this MZI, all the eight output ports ($O_1$-$O_8$) should be simultaneously monitored; in contrast, by exploiting on-chip monitoring only two CLIPPs ($A_7$ and $A_8$) need to be used. Similar considerations apply to any switching element whose output ports are not directly connected to external PDs.

In a second example, Figs 3(c)-(d) show the reconfiguration procedure to route signal $I_8$ to output ports $O_6$. Note that the optical signal at each stage is continuously monitored on-chip even after achieving the optimum tuning conditions, in order to assure robust locking of the MZI state against thermal crosstalk effects between adjacent actuated devices.

## V. On-Chip Channel Labelling and Discrimination

When multiple optical signals are simultaneously injected at different input ports of the switch fabric, CLIPP detectors can be used to identify channels coming from specific input ports regardless of the presence of other concurrent channels injected at the other input ports. However, in these conditions, both input ports of each MZI switch are fed with an optical signal, so that it is not possible to infer the MZI switching state by simply monitoring the light intensity of the two outputs. Signal labelling through pilot tones can be effectively exploited to make the CLIPP discriminate each input signals in such a way that reconfiguration of the whole circuit can be performed as in the single input case described in Sec. IV.

In a previous work, we have demonstrated that the CLIPP can indeed discriminate optical signals propagating through the same waveguide if these are labelled with a tone with an intensity modulation amplitude of a few percent and a

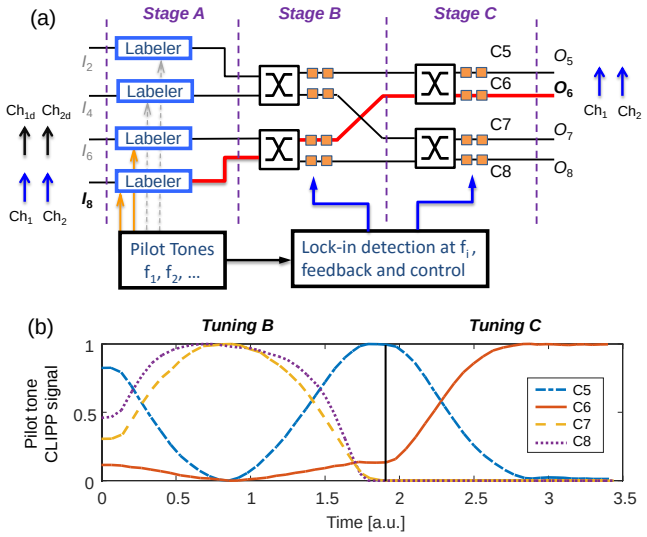


Fig. 4:CLIPP-assisted lightpath tracking of concurrent signals discriminated by using on-chip labelling through pilot tones. (a) MZIs of stage A are used as channel labeller adding a weak modulation tones at each input port. Two channels pairs are simultaneously injected at input ports $I_6$ ($Ch_{1d}$, $Ch_{2d}$) and $I_8$ ($Ch_1$, $Ch_2$) and labelled with tones $f_3$ = 10 kHz and $f_4$ = 7 kHz, respectively. (b) By demodulating the CLIPP signal at frequency $f_4$, channel pair $Ch_1$-$Ch_2$ can be can be monitored and routed through the switch fabric regardless of the presence of channel pair $Ch_{1d}$- $Ch_{2d}$.

frequency $f_i$ in the order of some kHz [29]. To identify the i-th channel, the CLIPP electric signal has to be demodulated twice, that is at the driving frequency $f_e$ of the CLIPP and at the modulation tone $f_i$. CLIPP assisted signal identification can be done without affecting the quality of the signal [30].

We demonstrate that the labelling operations can be performed directly on-chip. This enables to manage locally the channel identification, without any constraint on the transmission system used to generate the input channels. As shown in Fig. 4(a), the four MZIs of stage A are employed as slow thermal modulators to label channels coming from port $I_i$ with different tones $f_i$ ($k$ = 1, 2, 3, 4). The subsequent MZI switches are used to route the labelled signals through the 4x4 switch matrix identified by stages B and C. For clarity, in this section we maintain the same input port numbering as in Fig. 1(a), even though only even input ports are used.

To demonstrate lightpath tracking and broadband routing of concurrent signals, two channel pairs are simultaneously injected at two input ports of the switch fabric. Two signals $Ch_1$ and $Ch_2$, with carrier wavelengths $\lambda_{Ch1}$= 1558.2 nm and $\lambda_{Ch2}$= 1545.8 nm, and 10 Gbit/s on-off keying (OOK) modulation are injected at input port $I_8$. At input port $I_6$, concurrent channels $Ch_{1d}$ and $Ch_{2d}$ are injected, that are obtained by delaying and decorrelating $Ch_1$ and $Ch_2$ though a fiber span of a few km.

The pilot tones applied by on-chip labeler have a frequency $f_4$ = 7 kHz for $Ch_1$ and $Ch_2$, and $f_3$ = 10 kHz for $Ch_{1d}$ and $Ch_{2d}$. The MZI labelers are biased in the linear working point (3 dB attenuation) of their characteristic and introduce a peak-to-peak intensity modulation of about 5%.

As an example, let us consider the routing of both channels $Ch_1$- $Ch_2$ from input port $I_8$ to output port $O_6$. Fig. 4(b) shows the time-dependent signal provided by the four CLIPPs of stage C (C1 - C4) after demodulation at frequency $f_4$ of the channels

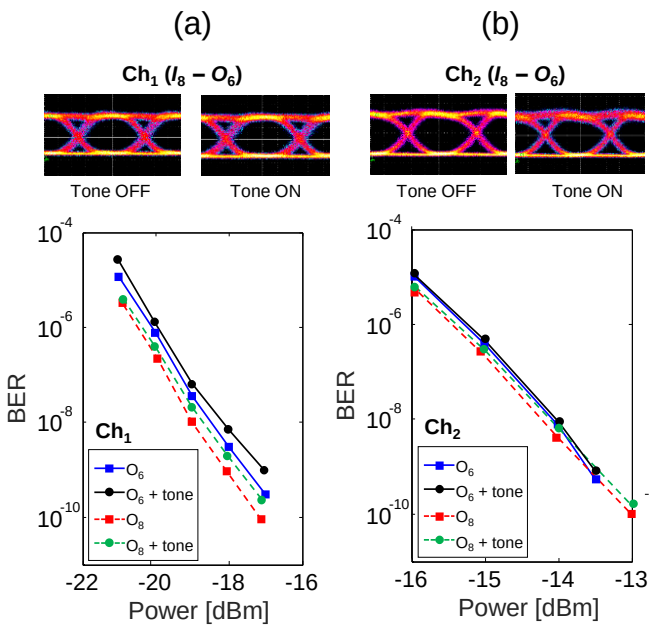


Fig. 5: Impact of the CLIPP-assisted light-path tracking and routing on the quality of concurrent channels discriminated by using on-chip labelling. The two 10 Gbit/s OOK signals Ch1 and Ch2 are modulated according to a $2^{31}$-1 pseudo random bit sequence (PRBS). (a) Top panel: eye diagrams of $Ch_1$ transmitted though the path $I_8$-$O_6$ with the pilot tone switched OFF (left) and ON (right). Bottom panel: BER curves measured along the paths $I_8$-$O_6$ (solid lines) and $I_8$-$O_8$ (dashed lines) with pilot tone switched OFF (squares) and ON (circles). (b) Eye-diagrams and BER curves of $Ch_2$ in the same cases considered in (a). No appreciable penalty is observed for both channels.

to be monitored and routed. First, the MZI of stage B is tuned to a switching state where the signals provided by C7 and C8 are minimized. Noteworthy, the presence of concurrent channels $Ch_{1d}$ and $Ch_{2d}$, that are routed towards C7 and C8, does not introduce significant crosstalk in the CLIPP signal. We evaluated that demodulation frequency mismatch, that is the CLIPP demodulation at a frequency different from that of the modulation tone, produces a very low crosstalk signal (lower than -50 dB), which is mainly due to the noise level of the electronic front-end. Therefore, this perturbation is 20 dB lower than the signal provided by a frequency matched CLIPP at the off-state port of a MZI with 30 dB optical extinction. This result is confirmed by the CLIPP signals measured after the tuning of stage C. In fact, the signal measured by $C_5$ (dominated by the optical crosstalk of frequency matched channels $Ch_1$-$Ch_2$ at port $O_5$) is even more pronounced than the signal provided by $C_7$ and $C_8$ (dominated by the frequency mismatched channels $Ch_{1d}$-$Ch_{2d}$)

We also evaluated the impact of on-chip channel labelling, discrimination and routing on the quality of the optical signals. Fig. 5 show the eye diagrams and bit-error rate measured on channels $Ch_1$ (a) and $Ch_2$ (b). The two channels are demultiplexed off-chip with a commercial free space tunable filter with a bandwidth of 0.3 nm. Eye diagrams shows that neither distortion nor eye opening reduction are observed when the MZI labelers are switched ON, in agreement with results obtained in the case of pilot tones applied through off-chip modulators [30]. This is confirmed by BER curves, performed for both channels routed along paths $I_8$ - $O_6$ and $I_8$ - $O_8$. For each path configuration, we routed the labelled channels by using pilot tones, then we compared the BER with the tones ON and after switching them OFF. As shown in the figure curves, no significant power penalties associated to the use of modulation tones was observed.

## VI. Active Compensation of Thermal Crosstalk

When tuning switch fabrics, the general approach is to create, during calibration tests, a look-up table that correlates the switching state of each element with the control signal required to tune it to the optimal working point [17]. This approach lacks of both flexibility and robustness since it cannot compensate dynamical temperature gradients, thermal crosstalk between elements, and ageing effects of the overall system. In this section, we demonstrate the effectiveness of the proposed feedback control tuning strategy to counteract mutual thermal crosstalk among the switching elements of the circuit.

Let us consider the case sketched in Fig. 6(a), where an optical signal coming from the stage *A* is routed by stages *B* and *C* to output port $O_8$. We focus on the performance of the bottom-most MZI switch of stage B, while several reconfiguration events occur in the switch fabric. In particular, we monitored the optical crosstalk induced when three surrounding MZIs (highlighted in green in the figure) randomly switch their state from ON to OFF condition. Since switching power of each MZI is about 10 mW (see Sec. II), this results in a total power ranging from 0 to 30 mW, with a variable combination of heat source position.

Figure 6(b) shows the time-dependent crosstalk at output port $O_6$ when the active thermal compensation of the MZI is OFF (green curve) and ON (blue curve). In this experiment the temperature of the entire silicon chip is stabilized with a thermo-electric cooler (TEC) inserted below the PCB. In the initial condition, the three surrounding MZIs are all switched off and a crosstalk signal of about -30 dB is measured. Then, the switching state of the three MZIs is randomly switched every 40 s. Without feedback control, the voltage on the MZI heater is kept constant. The crosstalk signal sharply increases after each circuit reconfiguration and, after some thermalization due to the TEC action, a residual steady-state optical crosstalk as high as -15 dB is observed. The blue curve demonstrates the effectiveness of active thermal compensation locally performed at the MZI site by using the CLIPP-assisted feedback control. An original optical crosstalk as low as -30 dB is rapidly recovered after the occurrence of every circuit reconfiguration. Noteworthy, Fig. 6(c) shows that the benefits of CLIPP-assisted control remain also if the TEC underneath the sample is switched off. This result suggests the possibility to exploit the proposed approach for the reconfiguration and control of uncooled silicon photonic circuits.

## VII. Conclusion

The paper reports on an extensive investigation of an 8x8 Silicon Photonic switch fabric based on Mach-Zehnder interferometers. Although the architecture is very well known, a new, original and deep insight on this circuit is presented. The main novelty is the use of non-invasive optical power monitor CLIPPs after each switching stage of the routing matrix. The 24 CLIPPs are interrogated by a multichannel electronic chip wire bonded to the photonic chip, enabling on-chip real-time

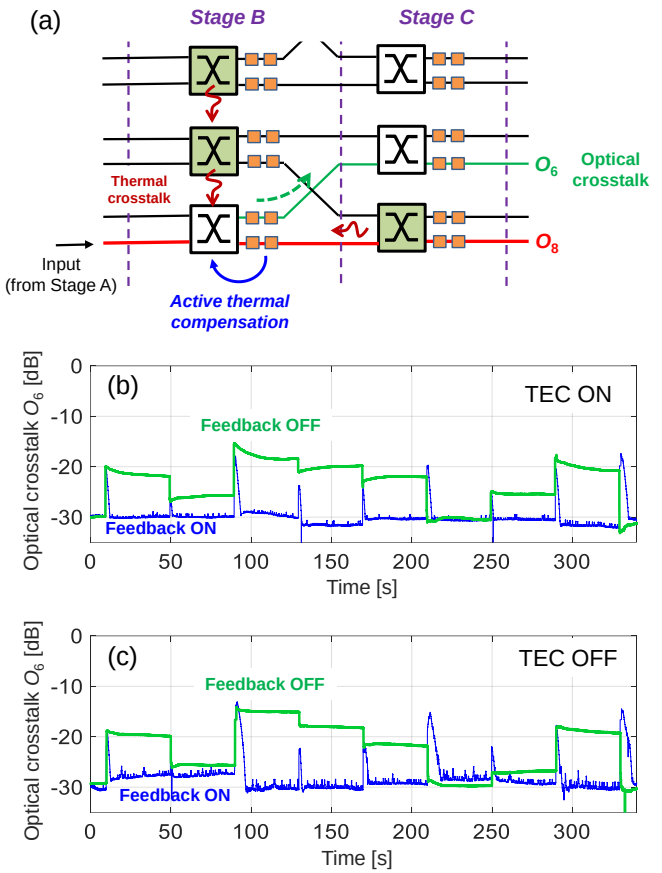


Fig. 6: CLIPP-assisted compensation of mutual crosstalk effects induced by the switching elements of the circuit. The control algorithm implements the additional moving average filter described in Sec. III to reduce residual fluctuations. (a) Schematic of the considered testbed: when the state of three surrounding MZI switches (highlighted in green) changes, thermal crosstalk modifies the switching state of the bottom-most MZI of stage *B* (biased to route the light to output $O_8$), thus inducing optical crosstalk at other output ports (for instance $O_6$). Panels (b) and (c) show the measured optical crosstalk at port $O_6$ during several random switching events of the three surrounding MZIs, when active thermal compensation is OFF (green curve) and ON (blue curve), when the silicon chip is cooled (b) and uncooled (c). In both cases, after every circuit reconfiguration, feedback control recover the original crosstalk level (-30 dB), whereas a steady-state crosstalk as high as -15dB is measured in open loop operation.

monitoring of the working state of the router. We have demonstrated the sequential tuning of the individual photonic elements to establish a routing path with local feedback control that exhibits also great robustness towards thermal crosstalk in different working conditions. The switching state of each MZI can be locally monitored and the feedback operates in real time regardless of the switching state of the other MZIs of the circuit, also without an external temperature stabilizer. In addition, neither previous calibration of the working points nor lookup tables are required; moreover, this approach is inherently insensible to channels power fluctuations.

Further, we have shown that the routing can be achieved with several WDM input signals simultaneously present at the same time simply by labeling the input physical channels with suitable pilot tones. The routing and the locking of the switching elements are achieved thanks to the selectivity of the CLIPP reading algorithm to the various labels with 10 Gbit/s WDM signals. Our approach is scalable to switch fabrics with higher port counts, different network-on-chip topologies as well as generic photonic integrated architectures.

## ACKNOWLEDGMENTS

The authors are grateful the staff of the James Watt Nanofabrication Centre (JWNC) at University of Glasgow for the fabrication of the Si samples and to A. Beretta (Linkra Microtech) and S. Masci (Politecnico di Milano) for the wire bonding of the silicon photonic chip.

## REFERENCES

[1] Roadmap of Photonic Systems Manufacturing Consortium (PSMC) www.photonicsmanufacturing.org
[2] D. A. B. Miller, "Designing Linear Optical Components" Opt. Photon. News 24(12), 38–38 (2013)
[3] F. Morichetti, S. Grillanda, and A. Melloni, "Toward feedback-controlled integrated photonics," IEEE Photon. J. 6, 1–6 (2014).
[4] K. Padmaraju, D. F. Logan, T. Shiraishi, J. J. Ackert, A. P. Knights, and K. Bergman, "Wavelength locking and thermally stabilizing microring resonators using dithering signals," J. Lightw. Technol. **32**, 505–515 (2014)
[5] Z. Yu, Li Yu, F. Shaoqi, A. W. Poon, "Towards Adaptively Tuned Silicon Microring Resonators for Optical Networks-on-Chip Applications," Selected Topics in Quantum Electronics, IEEE Journal of, vol. 20, no. 4, pp.136-149, July-Aug. 2014
[6] J.C.C. Mak, W.D. Sacher, X. Tianyuan, J.C. Mikkelsen, Y. Zheng, J.K.S. Poon, "Automatic Resonance Alignment of High-Order Microring Filters," Quantum Electronics, IEEE Journal of , vol.51, no.11, pp.1-11, Nov. 2015
[7] H. Jayatilleka, K. Murray, M.Á. Guillén-Torres, M. Caverley, R. Hu, N. A.F. Jaeger, L. Chrostowski, and S. Shekhar, "Wavelength tuning and stabilization of microring-based filters using silicon in-resonator photoconductive heaters," Opt. Express 23, 25084-25097 (2015)
[8] Yu Li and A.W. Poon, "Active resonance wavelength stabilization for silicon microring resonators with an in-resonator defect-state-absorption-based photodetector," Opt. Express **23**, 360-372 (2015)
[9] K. Padmaraju and K. Bergman, "Resolving the thermal challenges for silicon microring resonator devices," Nanophotonics 3(4), 269–281 (2014)
[10] J. A. Cox, A. L. Lentine, D. C. Trotter, and A. L. Starbuck, "Control of integrated micro-resonator wavelength via balanced homodyne locking," Opt. Express 22(9), 11279–11289 (2014)
[11] X. Zheng, E. Chang, P. Amberg, I. Shubin, J. Lexau, F. Liu, H. Thacker, S. S. Djordjevic, S. Lin, Y. Luo, J. Yao, J. H. Lee, K. Raj, R. Ho, J. E. Cunningham, and A.V. Krishnamoorthy, "A high-speed, tunable silicon photonic ring modulator integrated with ultra-efficient active wavelength control," Opt. Express 22(10), 12628–12633 (2014)
[12] C. Li, R. Bai, A. Shafik, E. Z. Tabasy, B. Wang, G. Tang, C. Ma, C. H. Chen, Z. Peng, M. Fiorentino, R. G. Beausoleil, P. Chiang, and S. Palermo, "Silicon photonic transceiver circuits with microring resonator bias-based wavelength stabilization in 65 nm CMOS," IEEE J. Solid-State Circuits 49(6), 1419–1436 (2014)
[13] P. Dong, Y. K. Chen, T. Gu, L. L. Buhl, D. T. Neilson, and J. H. Sinsky, "Reconfigurable 100Gb/s Silicon Photonic Network-on-Chip," J. Opt. Commun. Netw. 7(1), A37–A43 (2015)
[14] J. Fisher, A. Kodanev, M. Nazarathy, "Multi-Degree-of-Freedom Stabilization of Large-Scale Photonic-Integrated Circuits," J. Lightwave Technology, Vol. 33, 10, 2015
[15] B. Guha, A. Gondarenko, and M. Lipson, "Minimizing temperature sensitivity of silicon Mach-Zehnder interferometers," Opt. Express **18**, 1879–1887 (2010)
[16] B.G. Lee, N. Dupuis, P. Pepeljugoski, L. Schares, R. Budd, J.R. Bickford, and C.L. Schow, "Silicon Photonic Switch Fabrics in Computer Communications Systems," J. Lightwave Technol. 33, 768-777 (2015)
[17] C.P. Chen, et al., "Programmable Dynamically-Controlled Silicon Photonic Switch Fabric," J. Lightwave Technology, vol. PP, no. 99, 2015
[18] Q. Cheng, P. Stabile, Rohit, Abhinav, Wonfor, A., Penty, R.V., White, I.H. & Williams, Kevin (2015). First demonstration of automated control and assessment of a dynamically reconfigured monolithic 8×8 wavelength-and-space switch. Journal of Optical Communications and Networking, 7(3), A388-A395, 2015
[19] B. G. Lee, A. V. Rylyakov, W. M. Green, S. Assefa, C. W. Baks, R. Rimolo-Donadio, D. M. Kuchta, M. H. Khater, T. Barwicz, and C. Reinholm, "Monolithic silicon integration of scaled photonic switch fabrics, CMOS logic,

and device driver circuits," J. Lightwave Technol. 32, 743–751 (2014).
[20] Yu Li, Yu Zhang, Lei Zhang, and A.W. Poon, "Silicon and hybrid silicon photonic devices for intra-datacenter applications: state of the art and perspectives," Photon. Res. 3, B10-B27 (2015)
[21] L. Yang, Y. Xia, F. Zhang, Q. Chen, J. Ding, P. Zhou, and L. Zhang, "Reconfigurable non-blocking 4-port silicon thermo-optic optical router based on Mach-Zehnder optical switches," Opt. Lett. 40, 1402–1405 (2015)
[22] L. Lu, L. Zhou, Z. Li, X. Li, and J. Chen, "Broadband 4 × 4 nonblocking silicon electro-optic switches based on Mach-Zehnder interferometers," IEEE Photon. J. 7, 7800108 (2015)
[23] L. Chen and Y.-K. Chen, "Compact, low-loss and low-power 8 × 8 broadband silicon optical switch," Opt. Express 20, 18977–18985 (2012)
[24] N. Sherwood-Droz, H. Wang, L. Chen, B. G. Lee, A. Biberman, K. Bergman, and M. Lipson, "Optical 4 × 4 hitless silicon router for optical networks-on-chip (NoC)," Opt. Express 16, 15915–15922 (2008)
[25] L. Yang, H. Jia, Y. Zhao, and Q. Chen, "Reconfigurable nonblocking four-port optical router based on microring resonators," Opt. Lett. 40, 1129–1132 (2015)
[26] A. Biberman, B. G. Lee, N. Sherwood-Droz, M. Lipson, and K. Bergman, "Broadband operation of nanophotonic router for silicon photonic networks-on-chip," IEEE Photon. Technol. Lett. 22, 926–928 (2010)
[27] F. Morichetti, S. Grillanda, M. Carminati, G. Ferrari, M. Sampietro, M.J. Strain, M Sorel, A. Melloni, "Non-Invasive On-Chip Light Observation by Contactless Waveguide Conductivity Monitoring," Selected Topics in Quantum Electronics, IEEE Journal of, vol.20, no.4, pp.292,301, July-Aug. 2014
[28] P. Ciccarella, M. Carminati, G. Ferrari, D. Bianchi, S. Grillanda, F. Morichetti, A. Melloni and M. Sampietro, "Impedance Sensing CMOS Chip for Non-invasive Light Detection in Integrated Photonics," IEEE Trans. Circuits Syst. II, Exp. Briefs, in press.
[29] S. Grillanda, M. Carminati, F. Morichetti, P. Ciccarella, A. Annoni, G. Ferrari, M. Strain, M. Sorel, M. Sampietro, and A. Melloni, "Non-invasive monitoring and control in silicon photonics using CMOS integrated electronics," Optica 1, 129-136 (2014)
[30] S. Grillanda, F. Morichetti, N. Peserico, P. Ciccarella, A. Annoni, M. Carminati, A. Melloni, "Non-Invasive Monitoring of Mode-Division Multiplexed Channels on a Silicon Photonic Chip," J. Lightwave Technology, vol.33, no.6, pp.1197,1201, 2015
[31] M. Gnan, S. Thoms, D. S. Macintyre, R. M. De La Rue, and M. Sorel, "Fabrication of low-loss photonic wires in silicon-on-insulator using hydrogen silsesquioxane electron-beam resist," Electron. Lett. 44, 115–116 (2008)

**A. Annoni** received the M.Sc. in Telecommunications Engineering in 2011 from Politecnico di Milano (Italy) where he is currently pursuing a Ph.D. with the photonic devices group. His main research activity is focused on the implementation of the calibration and control layer for complex photonics integrated circuits.

**E. Guglielmi** received the B.Sc. cum laude in 2013 and the M.Sc. degree in electronic engineering in 2015 from Politecnico di Milano where he is currently pursuing a Ph.D. focused on the design of multichannel electronic platforms and digital algorithms for the control of complex photonic circuits.

**M. Carminati** (M'07) received the B.Sc. (in 2003) and M.Sc. (in 2005) degree in electronic engineering (both cum laude) from the Politecnico di Milano (Italy). In 2009 he completed the Ph.D. at DEIB - Politecnico di Milano, where he is currently a postdoctoral fellow (and contract professor since 2014) designing high-sensitivity impedance sensor and low-noise instrumentation. He has co-authored more than 70 peer-reviewed international publications, 6 book chapters and holds one patent.

**S. Grillanda** is a Postdoctoral researcher in the Photonic Devices Group at Politecnico di Milano since November 2014. He received from Politecnico di Milano the B.Sc. in 2008 and the M.Sc. cum laude in 2010 in Telecommunications Engineering, and the PhD Degree cum laude in 2014 in Information Technology Engineering. He has received the Honorable Mention at the 2015 Corning Outstanding Student Paper Competition at OFC 2015.

**P. Ciccarella** received the M.Sc. in electronic engineering cum laude in 2012 from Politecnico di Milano. In 2015 he completed his Ph.D. focused on the design and implementation of low-noise analog CMOS interfaces for innovative sensors.

**G. Ferrari** (M'98) received the Ph.D. degree from Politecnico di Milano in electronic engineering in 2003. Since 2005, he has been an Assistant Professor of electronics at Politecnico di Milano. The focus of his research activities is on the development of novel integrated instrumentation to probe electrical properties of materials and biosamples at the nanoscale. He has published more than 100 journal and conference papers, 7 chapter books and holds 4 patents.

**M. Sampietro** received the Master's degree in nuclear engineering in 1982 from Politecnico di Milano, where he is currently a Full Professor of electronic circuits and devices. He is responsible for the activities in high-sensitivity instrumentation for the nanoscience. He is the Coauthor of more than 200 peer-reviewed international publications. He has been a Vice dean of the Faculty and the Coordinator of many national and international research projects and scientific partner in five European projects.

**M. Sorel** received the Graduation degree (cum laude) in electrical and electronics engineering in 1995, and the Ph.D. degree in 1999 from Universita di Pavia. In 1998, he joined the Optoelectronics Research Group, University of Glasgow with a Rotary Foundation fellowship and was awarded a personal Marie-Curie fellowship in 1999 for research on integrated optical gyroscopes. He was appointed a Lecturer in 2002 and a Senior Lecturer in 2008. He has been engaged in research on semiconductor optoelectronics for more than 15 years. He has published more than 300 journal and conference papers.

**M. J. Strain** received the M.A.Sc. and Ph.D. degree in photonics from the University of Toronto and the University of Glasgow, respectively, in 2004 and 2008. He joined the Institute of Photonics at the University of Strathclyde as a Lecturer in photonic semiconductor devices in 2013. His research interests include photonic-integrated circuits for applications from all-optical signal processing and sensing, to cavity enhanced non-linear interactions.

**A. Melloni,** OSA Fellow, Full Professor at Politecnico di Milano - where he leads the group of Photonic Devices. With a background in microwaves, his field of research is in the analysis, design, characterization, control and exploitation of passive integrated optical devices for optical communication and sensing. He holds 13 international patents in the field of integrated optics and components and is author of over 90 publications on the major international journals.

**F. Morichetti** received the M.Sc. degree (cum laude) in telecommunications engineering in 2001 and the Ph.D. degree (cum laude) in information engineering in 2008 from Politecnico di Milano. In 2001 he joined the integrated optics lab of CoreCom, Italy. Since 2012, he has been a post-doc researcher at Politecnico di Milano. His research activity is focused on the modeling, design and characterization of photonic integrated circuits for optical signal processing. He is coauthor of 3 chapters of international books, more than 150 papers in international journals and conference proceedings, and 5 international patents.